Mon. Not. R. Astron. Soc. **000**, 1–9 (1998) Printed 19 April 1999 (MN LaTeX style file v1.4)

The non-Gaussian tail of cosmic-shear statistics

Guido Kruse & Peter Schneider
Max-Planck-Institut für Astrophysik, Postfach 1523, D-85740, Garching, Germany

ABSTRACT
Due to gravitational instability, an initially Gaussian density field develops non-Gaussian features as the Universe evolves. The most prominent non-Gaussian features are massive haloes, visible as clusters of galaxies. The distortion of high-redshift galaxy images due to the tidal gravitational field of the large-scale matter distribution, called cosmic shear, can be used to investigate the statistical properties of the LSS. In particular, non-Gaussian properties of the LSS will lead to a non-Gaussian distribution of cosmic-shear statistics. The aperture mass ($M_{\rm ap}$) statistics, recently introduced as a measure for cosmic shear, is particularly well suited for measuring these non-Gaussian properties. In this paper we calculate the highly non-Gaussian tail of the aperture mass probability distribution, assuming Press-Schechter theory for the halo abundance and the 'universal' density profile of haloes as obtained from numerical simulations. We find that for values of $M_{\rm ap}$ much larger than its dispersion, this probability distribution is closely approximated by an exponential, rather than a Gaussian. We determine the amplitude and shape of this exponential for various cosmological models and aperture sizes, and show that wide-field imaging surveys can be used to distinguish between some of the currently most popular cosmogonies. Our study here is complementary to earlier cosmic-shear investigations which focussed more on two-point statistical properties.

Key words: galaxies: clusters: general - cosmology: theory - dark matter - gravitational lensing

1 INTRODUCTION

The deflection of light due to the gravitational field of matter inhomogeneities is observable through the distortion of images of background galaxies. In the case of weak gravitational fields, i.e., in the absence of strong gravitational lensing effects like giant arcs, the images of a population of background sources with known intrinsic ellipticity distribution can be used to statistically investigate weak gravitational lensing effects by measuring a net ellipticity.

Cosmic shear – the line-of-sight integrated tidal gravitational field – reflects the statistical properties of the density fluctuation field (Gunn 1967, Blandford & Jaroszynski 1981). A quantitative description of this connection is given by the two-point correlation function of galaxy-image ellipticities, or by the rms-ellipticity within a (circular) aperture, which was investigated by several authors using the linear and nonlinear power spectrum of density fluctuations in different cosmologies (see the recent review by Mellier 1998, and references therein).

Schneider et al. (1998; hereafter SvWJK) investigated cosmic shear using the $M_{\rm ap}$-statistics which is a spatially filtered version of the projected density field. They computed the dispersion of $M_{\rm ap}$ for the linear and nonlinear power spectrum of density fluctuations in different cosmologies for a broad range of filter scales and showed that this quantity is a sensitive and 'local' measure of the power spectrum; in fact, as shown by Bartelmann & Schneider (1999), the mean-squared value of $M_{\rm ap}$ on an angular scale θ is a very good approximation to the power spectrum P_κ of the projected density field at a wavenumber $s \approx 4.25/\theta$. SvWJK calculated the skewness of $M_{\rm ap}$ in the frame of quasi-linear theory of structure growth and found that it is a sensitive indicator for the density parameter Ω_0, independent of the normalization of the power spectrum (see also Bernardeau, van Waerbeke & Mellier 1997; van Waerbeke, Bernardeau & Mellier 1999). The skewness measures the non-Gaussianity of the projected density field and indicates, according to its sign, an asymmetric positive or negative tail of the probability distribution function (PDF). The skewness of $M_{\rm ap}$, which reflects the skewness of the three-dismensional density fluctuations, was found to be positive, indicating an extended tail of the PDF towards high positive values of $M_{\rm ap}$. This behaviour is expected: the initial density contrast δ, which is assumed to be a Gaussian random field, becomes non-Gaussian during its evolution through gravitational collapse. That means the PDF of δ attains a cut-off near $\delta = -1$ and a broad positive tail, according to the occurrence of underdense and overdense regions. Since $M_{\rm ap}$ is a linear function of the projected density field, the PDF of $M_{\rm ap}$ is closely related to that of δ. Therefore the PDF of $M_{\rm ap}$ reflects the nonlinear evolution of δ.

The projected density field κ in general is defined as a projection of the three-dimensional density contrast δ, weighted by a redshift-dependent factor which accounts for the lensing geometry and the redshift distribution of the sources. The highest peaks of κ are expected to arise from physical objects with high three-dimensional density, i.e., collapsed haloes. In Kruse & Schneider (1999; hereafter KS99) we have calculated the number density of haloes which yield a value of $M_{\rm ap}$ larger than a certain threshold. We found that for all cosmologies considered, the number density of haloes above a threshold corresponding to a signal-to-noise of 5 exceeds ten per square degree, for currently feasible deep optical imaging, so that a wide-field deep optical survey should detect hundreds of such peaks, which can then be used to define a mass-selected sample of dark matter haloes (Schneider 1996).

In this paper we continue the investigation of statistical properties of the aperture mass by computing its cumulative probability distribution function (CPDF) for large positive values of $M_{\rm ap}$, assuming that all of these are caused by collapsed structures. Describing the density profile of the haloes by the universal mass profile found by Navarro, Frenk & White (1996, 1997; hereafter NFW), we can assign an angular cross-section to each halo. If this cross-section is integrated over the abundance of haloes as obtained from Press-Schechter theory, one can determine the probability to measure a value of $M_{\rm ap}$ larger than some threshold, i.e., the CPDF for the tail of $M_{\rm ap}$. Similar to the number density calculated in KS99, the amplitude and shape of this tail reflects the abundance of dark-matter haloes, which can be used as a powerful cosmological probe.

The rest of this paper is organized as follows: in Sect. 2 we briefly review the concept of the aperture mass, as applied to the NFW- profile. The cross-sectional area as a function of $M_{\rm ap}$, and the CPDF, are derived in Sect. 3, and results are given in Sect. 5. The number density of peaks in the two-dimensional distribution of $M_{\rm ap}$ will be strongly affected, though in a controllable way, by noise, mainly coming from the intrinsic ellipticity distribution of galaxies. We consider an alternative observable for the abundance of peaks in $M_{\rm ap}$ in Sect. 4. Finally, we summarize and discuss our results in Sect. 6.

2 FORMALISM

Following Schneider (1996), we define the spatially filtered mass inside a circular aperture of angular radius θ around the point $\boldsymbol{\zeta}$,

$$M_{\rm ap}(\boldsymbol{\zeta}) := \int {\rm d}^2\vartheta\ \kappa(\boldsymbol{\vartheta})\ U(|\boldsymbol{\vartheta}-\boldsymbol{\zeta}|), \tag{1}$$

where the continuous weight function $U(\vartheta)$ vanishes for $\vartheta > \theta$. If $U(\vartheta)$ is a compensated filter function,

$$\int_0^\theta {\rm d}\vartheta\ \vartheta\ U(\vartheta) = 0, \tag{2}$$

one can express $M_{\rm ap}$ in terms of the tangential shear $\gamma_{\rm t}(\boldsymbol{\xi};\boldsymbol{\zeta})$ at position $\boldsymbol{\xi}+\boldsymbol{\zeta}$ relative to the point $\boldsymbol{\zeta}$

$$M_{\rm ap}(\boldsymbol{\zeta}) = \int {\rm d}^2\xi\ \gamma_{\rm t}(\boldsymbol{\xi};\boldsymbol{\zeta})\ Q(|\boldsymbol{\xi}|), \tag{3}$$

where

$$\gamma_{\rm t}(\boldsymbol{\xi};\boldsymbol{\zeta}) = -{\rm Re}(\gamma(\boldsymbol{\xi}+\boldsymbol{\zeta})e^{-2i\phi}) \tag{4}$$

is the tangential component of the shear at relative position $\boldsymbol{\xi} = (\xi\cos\phi, \xi\sin\phi)$. The function Q is related to U by

$$Q(\vartheta) = \frac{2}{\vartheta^2}\int_0^\vartheta {\rm d}\vartheta'\ \vartheta'\ U(\vartheta')\ - U(\vartheta). \tag{5}$$

We use a filter function from the family given in SvWJK, specifically we choose that with $l=1$. Then writing $U(\vartheta) = u(\vartheta/\theta)/\theta^2$, and $Q(\vartheta) = q(\vartheta/\theta)/\theta^2$,

$$u(x) = \frac{9}{\pi}(1-x^2)\left(\frac{1}{3}-x^2\right), \tag{6}$$

and

$$q(x) = \frac{6}{\pi}x^2(1-x^2), \tag{7}$$

with $u(x)=0$ and $q(x)=0$ for $x>1$. We will describe the mass density of dark matter haloes with the universal density profile introduced by NFW,

$$\rho(r) = \frac{3H_0^2}{8\pi G}\ (1+z)^3\ \frac{\Omega_{\rm d}}{\Omega(z)}\ \frac{\delta_c}{r/r_{\rm s}(1+r/r_{\rm s})^2}, \tag{8}$$

with

$$\Omega(z) = \frac{\Omega_{\rm d}}{a+\Omega_{\rm d}(1-a)+\Omega_{\rm v}(a^3-a)},\ a = \frac{1}{1+z}. \tag{9}$$

$\Omega_{\rm d}$ and $\Omega_{\rm v}$ denote the present-day density parameters in dust and in vacuum energy, respectively. Haloes identified at redshift z with mass M are described by the characteristic density $\delta_{\rm c}$ and the scaling radius $r_{\rm s} = r_{200}/c$ where c is the concentration parameter (which is a function of $\delta_{\rm c}$) and r_{200} is the virial radius, defined such that a sphere with radius r_{200} has a mean interior density of 200 $\rho_{\rm crit}$ and contains the halo mass M_{200}. We compute the parameters which specify the density profile according to the description in NFW using the fitting formulae given there. The surface mass density of the NFW-profile is given by (see Bartelmann 1996)

$$\Sigma(\vartheta) = \frac{6H_0^2}{8\pi G}\ (1+z)^3\ \frac{\Omega_{\rm d}}{\Omega(z)}\ r_{\rm s}\ \delta_{\rm c}\ f\left(\frac{\vartheta}{\theta_{\rm s}}\right), \tag{10}$$

with

$$f(x) = \frac{1}{x^2-1} \times \begin{cases} 1 - \dfrac{2}{\sqrt{1-x^2}}\ {\rm arctanh}\sqrt{\dfrac{1-x}{1+x}}, & \text{for } x<1 \\ 1 - \dfrac{2}{\sqrt{x^2-1}}\ {\rm arctan}\sqrt{\dfrac{x-1}{1+x}}, & \text{for } x>1 \end{cases}, \tag{11}$$

and $\theta_{\rm s} = r_{\rm s}/D_{\rm d}$. $D_{\rm d}$ is the angular diameter distance to the lens. Introducing the critical surface mass density

$$\Sigma_{\rm cr} = \frac{c^2}{4\pi G}\ \frac{D_{\rm s}}{D_{\rm d}D_{\rm ds}}, \tag{12}$$

with $D_{\rm s}$ and $D_{\rm ds}$ being the angular diameter distances to the source and that from the lens to the source, we can define the dimensionless surface density (convergence) which is a function of source redshift

$$\kappa(\vartheta, z_{\rm d}, z_{\rm s}) = \frac{\Sigma(\vartheta)}{\Sigma_{\rm cr}} = \kappa_0\ f\left(\frac{\vartheta}{\theta_{\rm s}}\right), \tag{13}$$

with

$$\kappa_0 = 3\,(1+z)^3\,\frac{\Omega_{\rm d}}{\Omega(z)}\,r_{\rm s}\,\frac{H_0^2}{c^2}\,\delta_c\,\frac{D_{\rm d}D_{\rm ds}}{D_{\rm s}}. \qquad (14)$$

We assume a normalized source redshift distribution of the form

$$p_z(z) = \frac{\beta}{z_0^3\,\Gamma\left(\frac{3}{\beta}\right)}\,z^2\,\exp(-[z/z_0]^\beta), \qquad (15)$$

(see Brainerd et al. 1996). The mean redshift of this distribution is proportional to z_0 and depends on the parameter β which describes how quickly the distribution falls off towards higher redshifts. We will use the values $\beta = 1.5$ and $z_0 = 1$. For these values the mean redshift $\langle z\rangle$ is given by $\langle z\rangle = 1.505\,z_0$. With the distribution (15) we define a source distance-averaged surface density

$$\kappa(\vartheta, z_{\rm d}) = \int {\rm d}z_{\rm s}\;p_z(z_{\rm s})\;\kappa(\vartheta, z_{\rm d}, z_{\rm s}) = \bar\kappa_0\;f\left(\frac{\vartheta}{\theta_{\rm s}}\right), \qquad (16)$$

with $\bar\kappa_0 = \int {\rm d}z_{\rm s}\;p_z(z_{\rm s})\;\kappa_0$. Inserting (16) in (1) we get, after introducing polar coordinates for $\boldsymbol{\vartheta}$ and setting $\boldsymbol{\zeta} = (\zeta, 0)$, which is the radial distance of the aperture centre from the halo center,

$$M_{\rm ap}(\zeta) = \int_{\max(0,\zeta-\theta)}^{\zeta+\theta} {\rm d}\vartheta\;\vartheta\;\kappa(\vartheta) \times \int_{-\phi_{\rm m}}^{\phi_{\rm m}} {\rm d}\phi\;U\left(\sqrt{\vartheta^2+\zeta^2-2\vartheta\zeta\cos(2\phi)}\right), \qquad (17)$$

where $\phi_{\rm m} = \min\left(\pi, \arccos\left(\frac{\vartheta^2+\zeta^2-\theta^2}{2\vartheta\zeta}\right)\right)$. For the filter function chosen above , the ϕ-integration can be performed analytically.

In Figure 1 we plot the aperture mass of a halo with mass $M = 10^{15} M_\odot/h$ at redshift $z_{\rm d} = 0.3$ as a function of the radial distance ζ, using a filter scale of $\theta = 2'$, for five cosmological models. If we fix the parameters $(M, z_{\rm d}, \theta)$, the aperture mass is a monotonically decreasing function of ζ between $\zeta = 0$ and the first root of $M_{\rm ap}$.

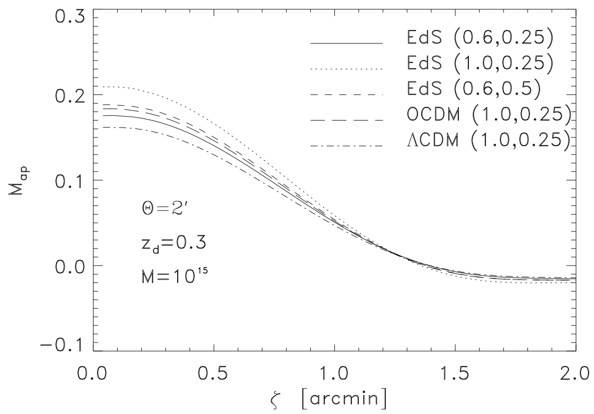

Figure 1. The aperture mass, as defined in (17), as a function of the radial distance ζ computed for five different cosmologies as indicated by the line types. The numbers in parentheses are the normalization σ_8 annd the shape parameter Γ. The halo mass is $10^{15} M_\odot/h$ and its redshift $z_{\rm d} = 0.3$. The filter radius is $\theta = 2$ arcmin.

3 THE TAIL OF $M_{\rm AP}$-STATISTICS

In this section we calculate the CPDF $P(> M_{\rm ap}, \theta)$, i.e., the probability to find an aperture mass larger than $M_{\rm ap}$ using a filter with radius θ. We concentrate on values of $M_{\rm ap}$ which are much larger than the rms value of $M_{\rm ap}$, i.e., we consider only the far tail of the probability distribution. We may assume that such high values of $M_{\rm ap}$ are caused exclusively by collapsed haloes. Thus, from the properties of such haloes, together with their abundance, we can then determine the CPDF.

Assuming a halo characterized by its mass M and redshift $z_{\rm d}$, we can invert the function (17) for a given value of $M_{\rm ap}$ and a fixed filter radius θ (see Fig. 1). As a result we get the separation $\zeta = \zeta(M_{\rm ap}, \theta, M, z_{\rm d})$. Owing to the monotonic behaviour of $M_{\rm ap}$ between $\zeta = 0$ and its first root, separations smaller than the one obtained by inversion correspond to aperture masses larger than the threshold $M_{\rm ap}$. Therefore, ζ defines for each halo an angular cross section

$$\sigma(M_{\rm ap}, \theta, M, z_{\rm d}) := \pi\;\zeta^2(M_{\rm ap}, \theta, M, z_{\rm d}), \qquad (18)$$

which represents the halo target area for detecting a weak lensing signal with an aperture mass larger than $M_{\rm ap}$. The cross section (18) is non-zero if the aperture mass measured in the halo centre is larger than the threshold $M_{\rm ap}$ (see Fig. 1).

The CPDF is now obtained by summing up the cross sections of all haloes within a unit solid angle; this yields

$$P(> M_{\rm ap}, \theta) = \frac{c}{H_0}\int {\rm d}z_{\rm d}\;\frac{(1+z_{\rm d})^2}{E(z_{\rm d})}\;D_{\rm d}^2(z_{\rm d}) \times \int {\rm d}M\;N_{\rm halo}(M, z_{\rm d})\;\sigma(M_{\rm ap}, \theta, M, z_{\rm d}), \qquad (19)$$

with

$$E(z_{\rm d}) = \sqrt{\Omega_{\rm d}(1+z_{\rm d})^3 + (1-\Omega_{\rm d}-\Omega_{\rm v})(1+z_{\rm d})^2 + \Omega_{\rm v}}. \qquad (20)$$

$N_{\rm halo}(M, z_{\rm d})\,{\rm d}M$ is the comoving number density of haloes with mass within ${\rm d}M$ about M at redshift $z_{\rm d}$. We assume that $N_{\rm halo}(M, z_{\rm d})$ can be obtained from Press and Schechter (1974) theory (see, e.g. Lacey & Cole 1993, 1994). The M-integral in (19) extends from a lower threshold $M_{\rm t}$ to infinity, where σ vanishes for $M \le M_{\rm t}$ (see KS99).

4 NUMBER DENSITY OF HALOES, SELECTED BY $M_{\rm AP}$ AND SIZE

In KS99, we have calculated the number density of haloes $N(> M_{\rm ap}, \theta)$ with an aperture mass $> M_{\rm ap}$, using the same physical model as described above. Considering $M_{\rm ap}(\theta)$ as a two-dimensional map, $N(> M_{\rm ap}, \theta)$ yields, at fixed filter scale θ, the number density of peaks in this map with amplitude $> M_{\rm ap}$. Such peaks may be generated by noise where the major contribution comes from the intrinsic ellipticity distribution of galaxies. Intuitively, one might expect that high peaks are less effected by noise than smaller ones; this motivates us to consider the number density of haloes with aperture mass $> M_{\rm ap}$ and cross-sectional area

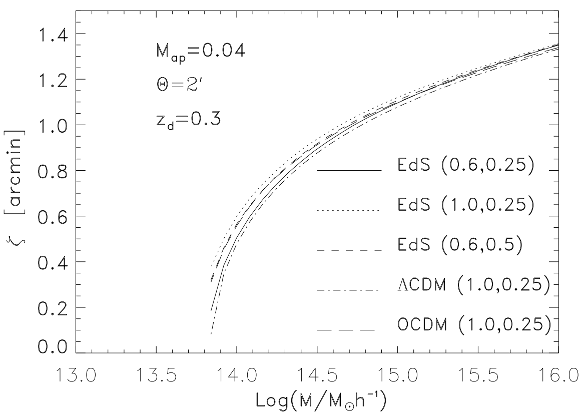

Figure 2. The cross section radius obtained from inverting (17) as a function of the lens mass for the same cosmological models as in Figure 1. (17) is inverted for the aperture mass $M_{\rm ap} = 0.04$, a filter radius $\theta = 2$ arcmin and a halo redshift $z_{\rm d} = 0.3$. The cross section of haloes characterized by the fixed parameters written in the panel is zero for halo masses smaller than $M_{\rm t} \sim 10^{13.8} M_\odot/h$.

$> \sigma = \pi\zeta_{\rm t}^2$, which is again obtained from summing over all haloes per unit solid angle,

$$N(> M_{\rm ap}, > \zeta_{\rm t}, \theta) = \frac{c}{H_0} \int {\rm d}z_{\rm d}\, \frac{(1+z_{\rm d})^2}{E(z_{\rm d})}\, D_{\rm d}^2(z_{\rm d}) \times \int {\rm d}M\; N_{\rm halo}(M, z_{\rm d})\; {\rm H}[\zeta(M_{\rm ap}, \theta, M, z_{\rm d}) - \zeta_{\rm t}], \qquad (21)$$

where H is the Heaviside step function. The integrand is non-zero only for $M > M_{\rm t}$, where $M_{\rm t} = M_{\rm t}(\zeta_{\rm t}, z_{\rm d}, M_{\rm ap}, \theta)$ is the mass obtained by inversion of the function shown in Fig. 2. For $\zeta_{\rm t} = 0$, $N(> M_{\rm ap}, > \zeta_{\rm t}, \theta) = N(> M_{\rm ap}, \theta)$. The value of $\zeta_{\rm t}$ for which $N(> M_{\rm ap}, > \zeta_{\rm t}, \theta)$ decreases to about 1/2 of $N(> M_{\rm ap}, \theta)$ yields the characteristic size of peaks corresponding to a given $M_{\rm ap}$; this value is expected to be $< \theta$. E.g., for the EdS(0.6,0.25) cosmology we obtain $N(> 0.04, > 0.45', 2') = 4.6$ which can be compared to $N(> 0.04, 2') = 9.4$ computed in KS99. For this example the characteristic size of a peak is roughly 1/4 of the filter radius.

5 RESULTS

In this section we consider $P(> M_{\rm ap}, \theta)$ for different cosmological models in the regime where the PDF of $M_{\rm ap}$ describes the non-linear evolution of the density field. Furthermore, we use the observable (21) to get additional constraints for the cosmological parameters. We perform our calculations for the same five cosmological models as shown in Figure 1. For three of them, the power spectrum is approximately cluster normalized, which corresponds to $\sigma_8 \approx 0.6$ for an Einstein-de Sitter universe (EdS, $\Omega_{\rm d} = 1$, $\Omega_{\rm v} = 0$) and $\sigma_8 = 1$ for both an open universe (OCDM, $\Omega_{\rm d} = 0.3$, $\Omega_{\rm v} = 0$) and a spatially flat universe with cosmological constant (ΛCDM, $\Omega_{\rm d} = 0.3$, $\Omega_{\rm v} = 0.7$). For these models we use the shape parameter $\Gamma = 0.25$ which yields the best fit to the observed two-point correlation function of galaxies (Efstathiou 1996). The remaining two EdS models have higher normalization ($\sigma_8 = 1$, approximately corresponding to COBE normalization) or a different shape parameter ($\Gamma = 0.5$).

In the absence of lensing, the expectation value of $M_{\rm ap}$ vanishes, and its dispersion depends on the intrinsic ellipticity distibution, as calculated in Schneider (1996),

$$\sigma_{\rm c}(\theta) = 0.016 \left(\frac{n}{30\ {\rm arcmin}^{-2}}\right)^{-1/2} \left(\frac{\sigma_\epsilon}{0.2}\right) \left(\frac{\theta}{1'}\right)^{-1}. \qquad (22)$$

We take $n = 30\ {\rm arcmin}^{-2}$ and $\sigma_\epsilon = 0.2$ for the number density of background galaxies and their intrinsic ellipticity distribution, respectively, as representative values in the following. The signal-to-noise ratio of $M_{\rm ap}$ is then defined as

$$S_{\rm c}(\theta) = \frac{M_{\rm ap}(\theta)}{\sigma_{\rm c}(\theta)}. \qquad (23)$$

In Fig. 3 we plot the probability (19) for four different filter scales for the cosmologies introduced in the beginning of this section, for values of $M_{\rm ap}$ between M_0 and $2M_0$, where the value of M_0 was chosen to correspond to a signal-to-noise ratio of five, $M_0 = 5\sigma_{\rm c}(\theta)$. According to this figure the probability $P(> M_{\rm ap}, \theta)$ can be well approximated by an exponential,

$$P(> M_{\rm ap}, \theta) = p_0\, \exp\left[-\frac{(M_{\rm ap} - M_0)}{c}\right], \qquad (24)$$

where p_0 and c are fit parameters. From (24) it is clear that p_0 is the probability to find a value of $M_{\rm ap}$ larger than M_0. We determined p_0 and c simply by assuming that the logarithm of $P(> M_{\rm ap}, \theta)$ in the interval $[M_0, 2M_0]$ follows a straight line. The maximal relative deviation between the probability (19) and its approximation (24) in Fig. 3 is about 3 percent.

If we compute the probability according to the approximation (24), all information on cosmology is contained in the parameters p_0 and c. If we attempt to constrain the cosmological parameter set, we have to compute dispersions for the fit parameters. In the following we employ a maximum likelihood analysis to derive confidence levels in the parameter space $\{c, p_0\}$.

In order to obtain a likelihood function we have to specify a probability distribution for finding a particular set of values $\{M_{\rm ap}^{\rm i}\}$, ${\rm i} \in [1, N_{\rm f}]$ of $N_{\rm f}$ statistically independent aperture mass values. As an example, we shall assume that we have an image with side length L. SvWJK showed that about $N_{\rm f} = (L/(2\theta))^2$ statistically independent fields can be placed on the image. This means that we consider two fields to be statistically independent if their angular separation is about two filter radii since then the correlation coefficient of the two fields is below 1 percent (see SvWJK). We suppose that this sample contains $N_>$ values of $M_{\rm ap}$ which are above the threshold M_0. This subsample consists of aperture mass values $M_{\rm ap}^{\rm j} > M_0$, ${\rm j} \in [1, N_>]$. Now we may ask for the probability to find $N_> \in [1, N_{\rm f}]$ values above the threshold if we have a sample of $N_{\rm f}$ fields. For each of the $N_{\rm f}$ aperture mass measurements the event $M_{\rm ap} > M_0$ is supposed to occur with probability p_0. Obviously this random process can be described by a binomial distribution,

$$P(N_>|N_{\rm f}, p_0) = \binom{N_{\rm f}}{N_>}\, p_0^{N_>}\, (1-p_0)^{N_{\rm f}-N_>}. \qquad (25)$$

Of course, we can hope to estimate the two parameters p_0 and c only for observations for which $N_> \gg 1$; in particular,

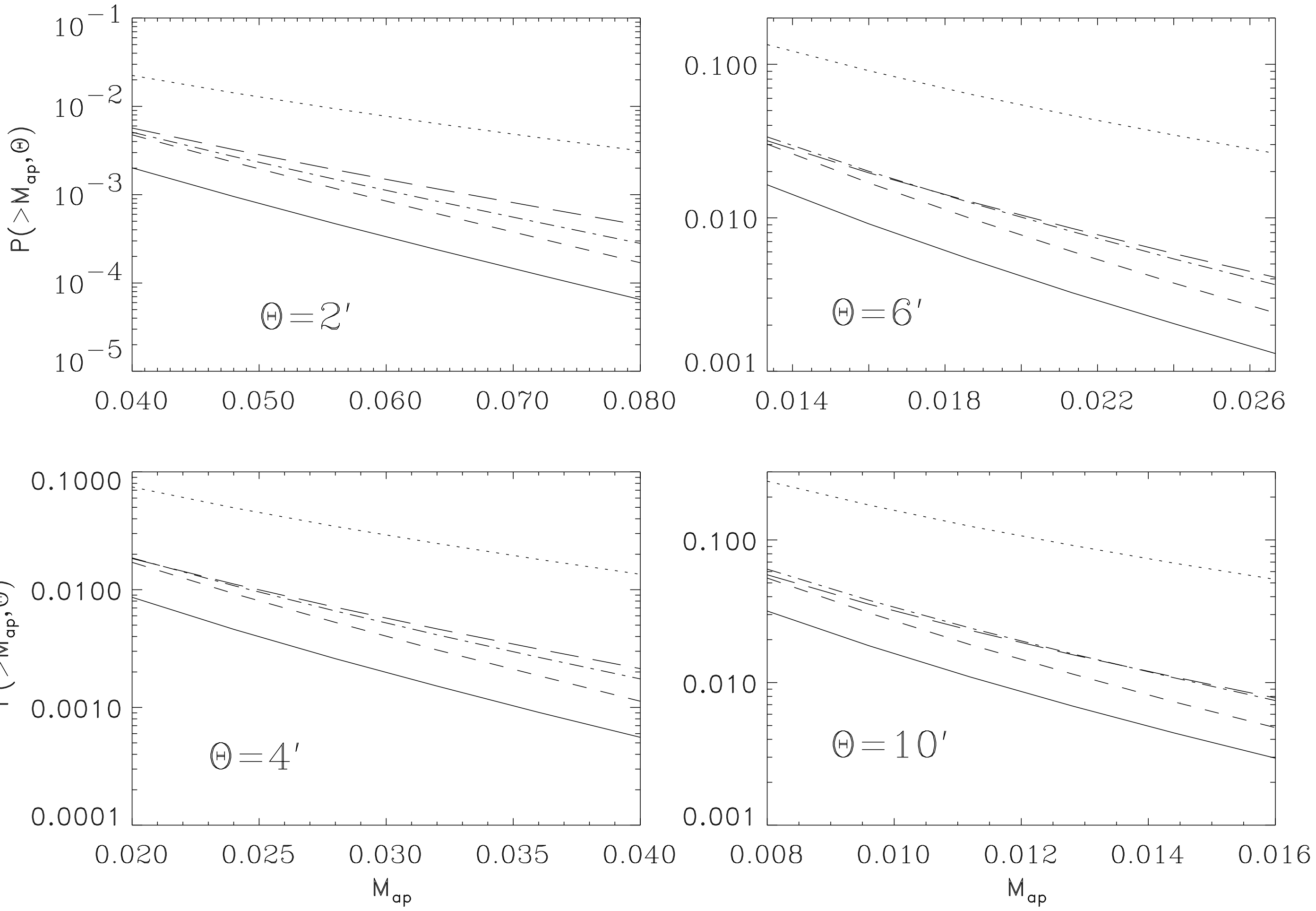

Figure 3. The probability as defined in (19) for the filter radii $\theta = 2, 4, 6, 10$ arcmin. In each panel we plot the same cosmological models as indicated in Figs. 1 and 2. The aperture mass range is defined by $[M_0, 2M_0]$, where $M_0 = 5 \cdot \sigma_{\rm c}(\theta)$ [see (23) and (22)].

if $N_> = 0$, the parameter c will be completely undetermined. Thus, we want to consider only realizations of (25) with $N_> \geq 1$, and therefore renormalize $P(N_>|N_{\rm f}, p_0)$,

$$f \sum_{N_>=1}^{N_{\rm f}} P(N_>|N_{\rm f}, p_0) = 1, \qquad (26)$$

where

$$f = \frac{1}{1-(1-p_0)^{N_{\rm f}}}. \qquad (27)$$

In addition, we consider the probability distribution of $M_{\rm ap}$ itself for values above the threshold M_0. The normalized PDF of $M_{\rm ap} \geq M_0$ can be obtained from (24) by

$$\begin{aligned}\hat{p}(M_{\rm ap}) &= \frac{1}{p_0}\left|\frac{{\rm d}}{{\rm d}M_{\rm ap}}P(>M_{\rm ap},\theta)\right| \\ &= \frac{1}{c}\exp\left[-\frac{(M_{\rm ap}-M_0)}{\rm c}\right]. \qquad (28)\end{aligned}$$

Combining both probabilities, we obtain the likelihood function

$$\mathrm{L}(M_{\rm ap}^1, ..., M_{\rm ap}^{N_>}|p_0, c) = P(N_>|N_{\rm f}, p_0) \prod_{\rm j=1}^{N_>} \hat{p}(M_{\rm ap}^{\rm j}), \qquad (29)$$

which describes the probability to find $N_>$ aperture masses $> M_0$ where those above the threshold follow the distribution (28). From (29) we can derive maximum likelihood estimates for both fit parameters. Denoting these estimates by $(\hat{c}, \hat{p}_0)$ we obtain by differentiating (29) w.r.t. c and p_0

$$\hat{c} = \frac{1}{N_>} \sum_{j=1}^{N_>} M_{\rm ap}^{\rm j} - M_0 \qquad (30)$$

and

$$\hat{p}_0 = \frac{N_>}{N_{\rm f}}; \qquad (31)$$

these results are of course not unexpected. In order to show that (30) and (31) are unbiased estimators we have to evaluate their ensemble average which can be performed by applying the operator

$$\begin{aligned}\mathrm{P}(X) &= f \sum_{N_>=1}^{N_{\rm f}} \binom{N_{\rm f}}{N_>} p_0^{N_>} (1-p_0)^{N_{\rm f}-N_>} \\ &\times \prod_{\rm j=1}^{N_>} \int_{M_0}^{\infty} {\rm d}M_{\rm ap}^{\rm j}\, \hat{p}(M_{\rm ap}^{\rm j})\ (X). \qquad (32)\end{aligned}$$

Averaging (30) and (31) with (32) yields

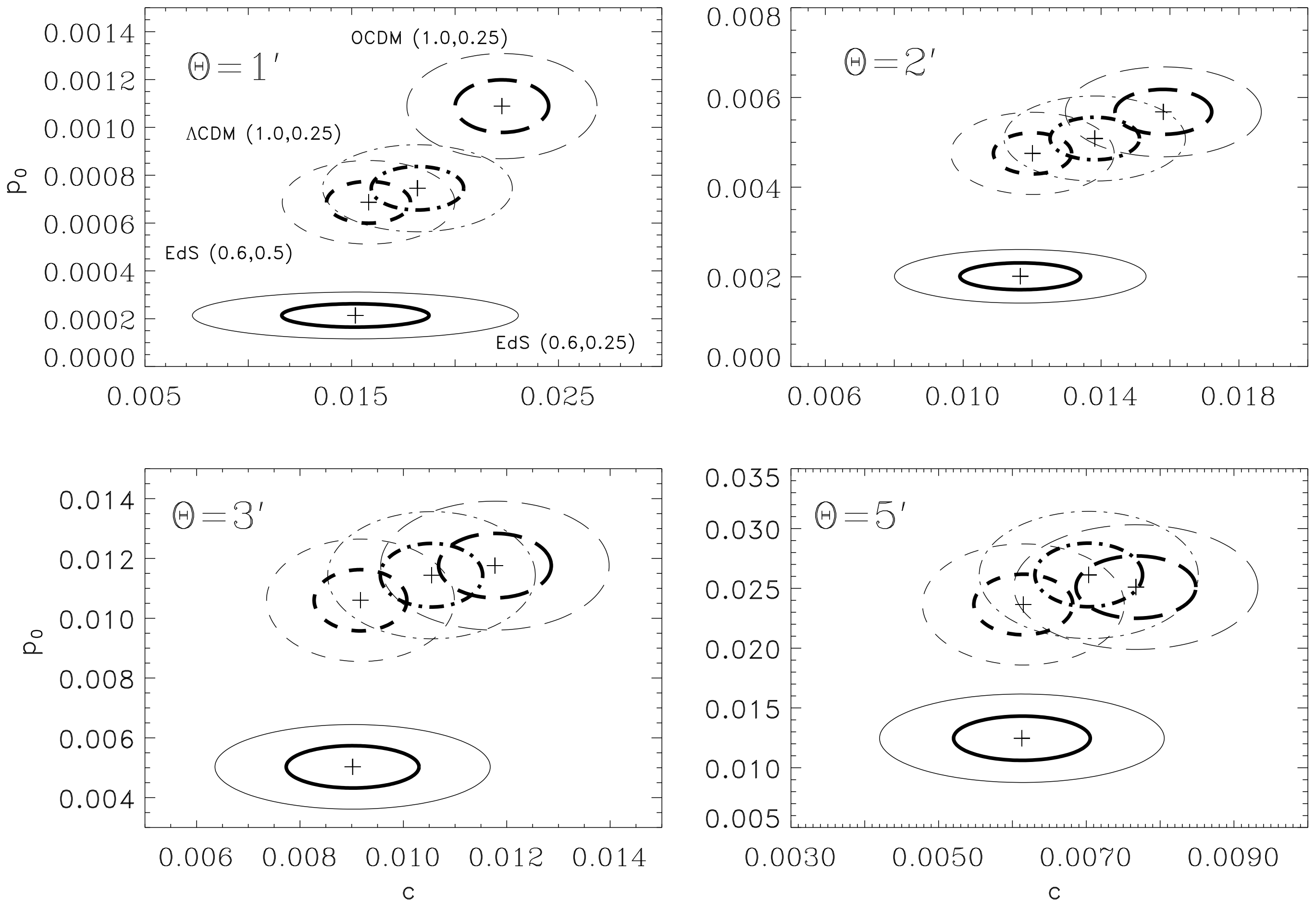

Figure 4. The fit parameters of the exponential (24) denoted by crosses computed as described in the text together with their 1-σ error ellipses which are defined by the dispersions (39) and (40). For all panels the signal-to-noise ratio threshold M_0/σ_c is 5. Haloes with redshift in $z_d \in [0,1]$ are considered. We use the source redshift distribution (15) with $\beta = 1.5$ and $z_0 = 1$. The thin and the thick curves describe a 25 deg^2 and a 100 deg^2 survey, respectively. The cosmological models are indicated in the upper left panel. The different panels are obtained by varying the filter scale, $\theta = 1, 2, 3, 5$ arcmin. We do not plot the EdS(1.0,0.25) models because it is well separated from the other cosmologies (p_0 is about a factor of 5 larger compared to the probabilities of the remaining model).

$$\langle \hat{c} \rangle = \mathrm{P}(\hat{c}) = c \text{ and } \langle \hat{p}_0 \rangle = \mathrm{P}(\hat{p}_0) = p_0 f. \tag{33}$$

Because of the second of eqs.(33), $\hat{p}_0$ is an unbiased estimator for p_0 only if $f \approx 1$. In the following we will consider only values of p_0 and N_f which guarantee that $f \approx 1$ is satisfied, otherwise the statistics is not good enough to determine the parameters accurately anyway. The correlation between the two estimators can be calculated from

$$\langle \hat{c}\ \hat{p}_0 \rangle = \mathrm{P}(\hat{c}\ \hat{p}_0) = c\ p_0\ f. \tag{34}$$

Since we have $f \approx 1$ these two estimators are not correlated. In the following we set $f = 1$.

Dispersions of the estimators are defined by

$$\sigma_{\hat{p}_0} = \sqrt{\langle \hat{p}_0^2 \rangle - \langle \hat{p}_0 \rangle^2} \tag{35}$$

and

$$\sigma_{\hat{c}} = \sqrt{\langle \hat{c}^2 \rangle - \langle \hat{c} \rangle^2}. \tag{36}$$

The calculation of the dispersions involves the application of the operator (32) to the squared estimators. After some algebra we obtain

$$\langle \hat{c}^2 \rangle = c^2 \left(1 + \sum_{N_>=1}^{N_\mathrm{f}} P(N_\mathrm{f}, p_0)\ N_>^{-1} \right) \tag{37}$$

and

$$\langle \hat{p}_0^2 \rangle = \frac{p_0}{N_\mathrm{f}}(1 - p_0) + p_0^2, \tag{38}$$

which together with (33) leads to

$$\sigma_{\hat{c}} = c \sqrt{\sum_{N_>=1}^{N_\mathrm{f}} P(N_> | N_\mathrm{f}, p_0)\ N_>^{-1}}, \tag{39}$$

and

$$\sigma_{\hat{p}_0} = \sqrt{\frac{p_0}{N_\mathrm{f}}(1 - p_0)}. \tag{40}$$

As expected, the rms values of the estimators decrease with increasing image size. This behaviour is obvious for (40) and can be seen for (39) if we use a recurrence relation to compute the binomial distribution for a given $N_>$. The offset for

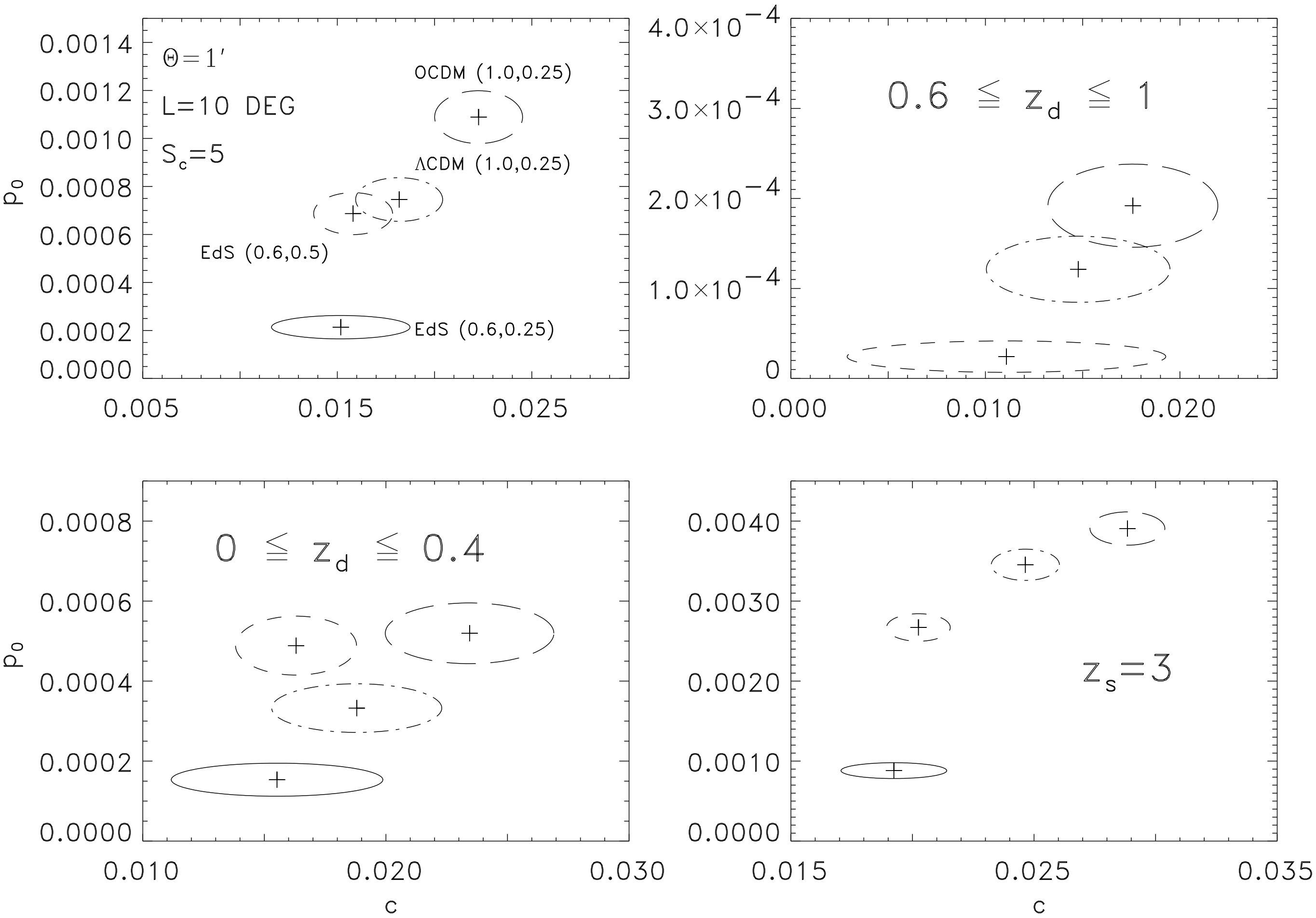

Figure 5. The top left plot is the same as in Fig. 4 for $L = 10$ deg. In the top right plot all parameters are unchanged but only halo redshifts $z_d \in [0.6, 1]$ are considered. The bottom left plot is the same as the top right one but halo redshifts are from the interval $z_d \in [0, 0.4]$. In the bottom right plot all sources are located at redshift $z_s = 3$; the other parameters are the same as in the top left plot. As in Fig. 4 we do not plot the high normalized EdS model which again is well separated from the other models. In the top right panel the value of p_0 for the EdS(0.6,0.25) model is so small that the normalization constant f differs from unity appreciably; we have therefore not included this model in the figure. The cosmological models are indicated in the upper left panel

the recurrence relation, $C(1) = N_f p_0 (1 - p_0)^{N_f - 1}$, rapidly decreases for large N_f and therefore the sum in (39).

Note that the rms values of the estimators depend only on their means and N_f which is determined by the image size for a given filter scale. Given that the mean values (c, p_0) depend on the filter radius θ and the threshold M_0 we can vary the parameter triple (θ, M_0, N_f) to obtain a significant difference between the various cosmological parameters. Furthermore, redshift information coming from possible redshift measurements of the haloes and the sources can be used to maximize the difference between various cosmologies.

In Fig. 4 we plot the mean values of the fit parameters (denoted by crosses) for the filter radii $\theta = 1, 2, 3, 5$ arcmin for four cosmological models. The threshold M_0 is defined by a signal-to-noise ratio of 5. For each cosmology and filter scale we use a 25 deg^2 (thin lines) and 100 deg^2 (thick lines) survey to compute the dispersions of the estimators (31) and (30) which define the 1-σ error ellipses in Fig. 4. As expected, if we double the side length of the image the dispersions of c and p_0 become smaller by about a factor of two. The COBE normalized EdS model is well separated for all filter scales. Since the probability p_0 in this model is about a factor of 5 larger than that of the remaining cosmologies we do not plot this model. The possibility of distinguishing cosmologies strongly depends on the filter scale. For an aperture with 1 arcmin filter radius we can clearly distinguish the EdS(0.6,0.25) and the low density model without cosmological constant from the other cosmologies if we use the survey with the larger area. If we enlarge the filter radius, the differences between the two low-density models and the EdS model with large shape parameter become smaller whereas the EdS(0.6,0.25) model remains distinguishable from all the other cosmologies.

In Fig. 5 we demonstrate the effects on the dispersions if we change the halo redshift integration range and the source redshift z_s, where we assume all sources to be located at the same redshift. For reference, we choose the upper left plot from Fig. 4 with $L = 10$ deg. If we shrink the halo redshift interval to $z_{\rm d} = [0.6, 1]$ we obtain the upper right plot. Because of the stronger evolution of the halo number density for high redshifts in the other cosmologies, the EdS(0.6,0.5) model can now be distinguished from the low-density models. The EdS(0.6,0.25) model has a value p_0 which is so small as to lead to a significant deviation of f – as defined in (27) – from unity, so that the expressions (39) and (40) are no longer valid, and therefore we have not plotted this model.

In the bottom left plot, compared to the upper right one, we only consider haloes having redshifts in the interval $z_{\rm d} = [0, 0.4]$. In this redshift range all cosmologies considered are distinguishable. The reason for the low-density models now being separated is the increasing difference between the rich cluster mass functions of both models if we choose smaller redshifts.

In the remaining plot, in comparison with the top left one, all sources are assumed to have the same redshift $z_{\rm s} = 3$ which is about twice the mean source redshift used in the other panels. Because of the improved efficiency of the weak lensing signal, the probability is increased by about a factor of 4. For this very deep survey all cosmologies are clearly separated. From Figs. 4 and 5 it becomes clear that we need large deep surveys in order to be able to distinguish clearly between the cosmological models considered, using only the statistics applied here.

If we want to compute $P(> M_{\rm ap}, \theta)$ as expected from real observations, we have to consider possible sources of error which may change the theoretical value of $M_{\rm ap}$, because the cross sections are given via aperture mass measurements (see Fig. 1). To account for the intrinsic ellipticity distribution of galaxies, we can proceed in the same way as for the observable $N(> M_{\rm ap}, \theta)$ in KS99. Essentially this means that we convolve $P(> M_{\rm ap}, \theta)$ with a Gaussian defined by the dispersion of the intrinsic galaxy ellipticity distribution of the sources. As explained in SvWJK, this dispersion is expected to dominate the noise in a measurement of $M_{\rm ap}$. The probability obtained from the convolution can be directly compared with observations. We have checked that, as expected from the results of KS99, the convolution only slightly enhances the theoretical values and does not change the shape of $P(> M_{\rm ap}, \theta)$ appreciably in the range of $M_{\rm ap}$ considered here. Therefore the fit formula we obtained remains valid, and the maximum likelihood method can be applied to derive dispersions for the fit parameters.

In Table 1 we show the number density of haloes with aperture mass larger than $M_{\rm ap} = 0.04$ and cross-section radii exceeding the threshold $\zeta_{\rm t} = 0.8$ arcmin for the filter radius $\theta = 2$ arcmin. According to the fact that the rich cluster mass function shows most clearly the cosmology dependence of the non-linear evolution of the density field and since cross-section radii above 0.8 arcmin correspond to the most massive non-linear objects (see Fig. 2), $N(> M_{\rm ap}, > 0.8', \theta)$ better distinguishes cosmologies than $N(> M_{\rm ap}, \theta)$ for the same $M_{\rm ap}$ and θ (see KS99). A drawback when using the observable (21) is the larger image size required for the detection of significant differences between various cosmologies. From the numbers in Table 1 we infer a survey area of 25 deg^2 which is needed to distinguish the cosmologies considered here significantly, i.e., with no overlapping Poissonian error bars.

Table 1. The number of haloes per square degree with aperture mass larger than $M_{\rm ap} = 0.04$ and cross-section radius greater than $\zeta_{\rm t} = 0.8$ arcmin, as defined in (21), computed for five cosmological models. The filter radius is $\theta = 2$ arcmin. The aperture mass and the dispersion determined by the filter radius correspond to a signal-to-noise ratio of 5.

Ω_0	Λ	Γ	σ_8	$N(> 0.8', > 0.04, 2')$
1.0	0	0.25	0.6	0.47
1.0	0	0.25	1.0	11.9
1.0	0	0.5	0.6	1.16
0.3	0	0.25	1.0	2.22
0.3	0.7	0.25	1.0	1.67

6 DISCUSSION AND CONCLUSIONS

In this paper we computed the highly non-Gaussian tail of the probability distribution of the aperture mass $M_{\rm ap}$ resulting from lensing by the large-scale structure. The CPDF is obtained by summing up the cross sections of dark matter haloes with assumed spherical mass density following a universal NFW density profile. We used Press-Schechter theory to compute the number density of massive haloes which cause the extended tail in the PDF of $M_{\rm ap}$.

The number density of haloes with large cross-sectional radii, or in other words, with large masses, is a sensitive measure for constraining the cosmological parameter set (see KS99, and references therein). We showed that the number density in a mass-selected sample of haloes with cross sectional radii above 0.8 arcmin, which corresponds to halo masses $\sim 10^{14} M_\odot/h$, is measureable in all cosmologies considered. Especially, from a deep, high-quality imaging survey of 25 deg^2, some of the currently most popular cosmologies can be distinguished by the varying number of haloes with the selected cross section threshold. The expected number of massive haloes varies from ~ 12 for the EdS(0.6,0.25) to ~ 300 for the high normalised EdS model if we use the above-mentioned survey.

The main result of this work is an analytical formula describing the PDF of the aperture mass, which turns out to be closely approximated by an exponential for values of $M_{\rm ap}$ well above its rms. This fact allows a simple maximum-likelihood analysis for distinguishing various cosmological models, using the non-Gaussian tail of $M_{\rm ap}$ only, as demonstrated in Sect. 5.

Modifications of the present investigation can well be imagined and may turn out to yield fruitful results in future. One is the use of (photometric) redshift estimates which allow a more precise measurement of the shear, owing to the redshift-dependent geometrical factors entering the projected surface mass density. If the haloes found by our method turn out to be associated with galaxy concentrations, their redshift can be estimated, and the halo abundance as a function of $M_{\rm ap}$ and redshift can be obtained, allowing to greatly refine the statistics considered here and in KS99.

Our approach to attempt measuring cosmological parameters is complementary to investigations employing two-point statistical measures, such as the rms shear in (circular) apertures or the shear two-point correlation function (e.g., Blandford et al. 1991; Kaiser 1992, 1998; Villumsen 1996; Jain & Seljak 1997; Bartelmann & Schneider 1999), and those which consider the skewness of cosmic shear statistics as a powerful handle on Ω_0 (e.g., Bernardeau et al. 1997; van Waerbeke et al. 1999; Jain et al. 1999). In contrast to these lower-order statistical measures, the highly non-Gaussian features of cosmic shear are expected to be less affected by noise, whose main contribution is the intrinsic ellipticity dispersion of source galaxies.

We note that the cosmology dependence of our results are mainly (but not exclusively) through the abundance of dark matter haloes as a function of mass and redshift. Thus, our statistics provides a fairly direct measure of this cluster abundance. In a future work, we shall attempt to relate $M_{\rm ap}$ to the true three-dimensional mass of haloes as determined in numerical N-body simulations, and thus relate the aperture mass statistics directly to the mass function of haloes.

It should be stressed that, whereas the aperture mass is most likely not the optimal statistics to measure the cosmic shear power spectrum (see Kaiser 1998, and Seljak 1998, for different approaches), it is a particularly convenient measure for highly non-Gaussian, spatially localized features which can be obtained locally and directly from the observed image ellipticities and whose noise properties can be straightforwardly investigated. In particular, cosmic shear measurement using $M_{\rm ap}$, and the search for mass-selected haloes (Schneider 1996; KS99) are just two aspects of the same underlying physics and statistics.

The validity of the various approximations which enter KS99 and the current study needs to be investigated in more detail. In a forthcoming paper (Reblinsky et al., in preparation) we will apply the aperture mass statistics to the same numerical simulations used in Jain et al. (1999), which combine very large N-body simulations with ray-tracing methods. Such numerical simulations are indispensible not only to assess the accuracy of the analytical approximation, but also to study statistical estimators which cannot be calculated analytically. Given the highly non-Gaussian nature of the projected density field resulting from the evolved LSS density distribution, it is by no means clear how to optimally and robustly distinguish between different cosmological models. The use of the far tail of the $M_{\rm ap}$-statistics should be viewed as one of several useful tools.

ACKNOWLEDGMENTS

This work was supported by the “Sonderforschungsbereich 375-95 für Astro-Teilchenphysik” der Deutschen Forschungsgemeinschaft. We want to thank B. Geiger and L. van Waerbeke for many interesting discussions, and M. Bartelmann for a careful reading of the manuscript.

REFERENCES

Bardeen, J.M., Bond, J.R., Kaiser, N. & Szalay, A.S. 1986, ApJ 304, 15
Bartelmann, M. 1996, A&A 313, 697
Bartelmann, M. & Schneider, P. 1999, A & A, in press, astro-ph/9902152
Bernardeau, F., van Waerbeke, L. & Mellier, Y. 1997, A&A 322, 1
Blandford, R.D. & Jaroszyński, M. 1981, ApJ 477, 27
Blandford, R.D., Saust, A.B., Brainerd, T.G. & Villumsen, J.V. 1991, MNRAS 251, 600
Brainerd, T.G., Blandford, R.D. & Smail, I. 1996, ApJ 466, 623
Efstathiou, G. 1996, in: *Cosmology and large scale structure*, Les Houches Session LX, R. Scheffer, J. Silk, M. Spiro & J. Zinn-Justin (eds.), North-Holland, p.133.
Gunn, J.E. 1967, ApJ 147, 61
Jain, B. & Seljak, U. 1997, ApJ 484, 560
Jain, B., Seljak, U. & White, S.D.M. 1998, astro-ph/ 9804238
Jain, B., Seljak, U. & White, S.D.M. 1999, astro-ph/ 9901191
Kaiser, N. 1992, ApJ 388, 272
Kaiser, N. 1998, ApJ 498, 26
Kruse, G. & Schneider, P. 1999, MNRAS 302, 821 (KS99)
Lacey, C. & Cole, S. 1993, MNRAS 262, 627
Lacey, C. & Cole, S. 1994, MNRAS 271, 676
Mellier, Y. 1998, preprint, To appear in Vol. 37 of *Annual Reviews of Astronomy and Astrophysics*
Mellier, Y., van Waerbeke, L. & Bernardeau, F. 1998, preprint
Navarro, J.F, Frenk, C.S. & White, S.D.M. 1996, ApJ 462, 563 (NFW)
Navarro, J.F, Frenk, C.S. & White, S.D.M. 1997, ApJ 490, 493 (NFW)
Press, W.H. & Schechter, P. 1974, ApJ 187, 425
Reblinsky, K., Kruse, G., Jain, B. & Schneider, P. 1999, in preparation
Schneider, P. 1996, MNRAS 283, 837
Schneider, P., van Waerbeke, L., Jain, B. & Kruse, G. 1998, MNRAS 296, 873 (SvWJK)
Seljak, U. 1998, ApJ 506, 64
van Waerbeke, L., Bernardeau, F. & Mellier, Y. 1999, A&A 342, 15
Villumsen, J. 1996, MNRAS 281, 369